Available online at www.sciencedirect.com
ScienceDirect
International Journal of Mass Spectrometry 261 (2007) 170–182
International Journal of Mass Spectrometry
www.elsevier.com/locate/ijms

Multiple scales analysis of early and delayed boundary ejection in Paul traps

N. Rajanbabu [a], Amol Marathe [b], Anindya Chatterjee [b], A.G. Menon [a,*]

[a] Department of Instrumentation, Indian Institute of Science, Bangalore 560012, India
[b] Department of Mechanical Engineering, Indian Institute of Science, Bangalore 560012, India

Received 20 July 2006; received in revised form 4 September 2006; accepted 4 September 2006
Available online 17 November 2006

Abstract

We use the method of multiple scales to elucidate dynamics associated with early and delayed ejection of ions in mass selective ejection experiments in Paul traps. We develop a slow flow equation to approximate the solution of a weakly nonlinear Mathieu equation to describe ion dynamics in the neighborhood of the stability boundary of ideal traps (where the Mathieu parameter $q_z = q_z^* = 0.908046$). The method of multiple scales enables us to incorporate higher order multipoles, extend computations to higher orders, and generate phase portraits through which we view early and delayed ejection.

Our use of the method of multiple scales is atypical in two ways. First, because we look at boundary ejection, the solution to the unperturbed equation involves linearly growing terms, requiring some care in identification and elimination of secular terms. Second, due to analytical difficulties, we make additional harmonic balance approximations within the formal implementation of the method.

For positive even multipoles in the ion trapping field, in the stable region of trap operation, the phase portrait obtained from the slow flow consists of three fixed points, two of which are saddles and the third is a center. As the q_z value of an ion approaches q_z^*, the saddles approach each other, and a point is reached where all nonzero solutions are unbounded, leading to an observation of early ejection.

The phase portraits for negative even multipoles and odd multipoles of either sign are qualitatively similar to each other and display bounded solutions even for $q_z > q_z^*$, resulting in the observation of delayed ejection associated with a more gentle increase in ion motion amplitudes, a mechanism different from the case of the positive even multipoles.

Keywords: 2D (linear) and 3D Paul traps; Nonlinear Mathieu equation; Multiple scales; Multipole superposition; Early, delayed ejection

1. Introduction

In this paper we study dynamics associated with early and delayed ejection observed in Paul traps operated in mass selective ejection mode. In particular, we study differences in the dynamics arising from higher order field superpositions of small magnitudes. The method of multiple scales is used to derive an approximate analytical expression which captures the slow variation in the amplitude of ion motion near the stability boundary.

Paul trap mass spectrometers consist of a three electrode mass analyzer with two end cap electrodes and a central ring electrode, all having hyperboloid geometry [1,2]. Ions of analyte gas, formed *in situ* by electron impact ionization, are trapped within the cavity by a trapping field formed by d.c. and rf potentials applied between the ring and end cap electrodes [1,3]. The motion of ions within an ideal trap is governed by two uncoupled, linear Mathieu equations [1,4] given by

$$\frac{\mathrm{d}^2u}{\mathrm{d}\tau^2} + (a_u + 2q_u \cos\, 2\tau)u = 0, \tag{1}$$

where u represents either the r (radial) or z (axial) direction of motion, $\tau = \Omega t/2$, where in turn Ω is the angular frequency of the rf drive applied to the central ring electrode, and t is time. In Eq. (1), a_u and q_u are Mathieu parameters which determine ion stability within the trap.

In mass selective ejection experiments, the trap is operated along the $a_z = 0$ axis (by setting the d.c. potential to 0) [5] of the Mathieu stability plot [3] and ions are destabilized from the trap by ramping the rf amplitude to cause the ion's q_z value to cross the stability boundary at or near $q_z^* = 0.908046$. In practical traps it is known that small field inhomogeneities, which arise due to geometric imperfections and experimental constraints,

* Corresponding author. Tel.: +91 80 2293 2487; fax: +91 80 2360 0135.
E-mail addresses: nrbabu@isu.iisc.ernet.in (N. Rajanbabu), amol@mecheng.iisc.ernet.in (A. Marathe), anindya100@gmail.com (A. Chatterjee), agmenon@isu.iisc.ernet.in (A.G. Menon).

1387-3806/$ – see front matter © 2006 Elsevier B.V. All rights reserved.
doi:10.1016/j.ijms.2006.09.009

cause ions to get ejected at smaller or larger q_z values (compared to $q_z^* = 0.908046$) resulting in the observation of early or delayed ejection, respectively. On account of this, it was observed very early during commercialization of the Paul trap mass spectrometer that traps were prone to errors in mass assignments [6], a problem that was subsequently overcome by increasing the distance between the two end cap electrodes. Wells et al. [7] showed that these mass shifts arise on account of the interplay of two primary factors which include (1) presence of nonlinear fields (caused by holes in the end caps as well as truncation of the electrodes) within the trap cavity which tends to delay ion ejection and (2) elastic and inelastic collisions of the ions with the bath gas which tend to shorten this delay. A recent report by Plass et al. [8] has provided further understanding on mass shifts through a study of its dependence on trap geometry, buffer gas, rf amplitude scan rate, ion mass and the chemical structure of the ion. In the context of the influence of field inhomogeneities causing delayed ion ejection Franzen and coworkers [9–12], in a series of numerical studies, showed that positive octopole and dodecapole superpositions cause ions to come out early (at $q_z < q_z^*$) and the presence of negative octopole and dodecapole superpositions or hexapole and decapole superpositions of either sign cause delayed ejection of ions (at $q_z > q_z^*$).

Understanding the dynamics associated with early and delayed ejection caused by field nonlinearities (inhomogeneities) is important in the context of newer trap geometries being investigated for their use as mass spectrometers. The 2D (linear) Paul trap, which consists of a four-rod assembly mass analyzer, has been used in both mass selective instability mode [13] as well as for resonance excitation experiments [14]. Modified geometries of 2D Paul traps with added octopole fields have also been investigated by Michaud et al. [15] and Collings [16]. Another direction of investigation concerns traps that have greatly simplified geometries compared to the hyperboloid geometry of the 3D Paul trap. An example of this is the cylindrical trap [17,18] which consists of a cylindrical ring electrode and two flat end cap electrodes, and has scope for MEMS scale fabrication [19,20]. Currently these instruments are being used as fieldable instruments [21] but we hope that better appreciation of the effects of multipole superpositions on boundary ejection of ions will help in developing miniaturized mass analyzers even for high performance applications. The common feature for all these mass analyzers is that the governing equations of ion motion within the trap cavity are Mathieu equations. Further, in these traps, on account of non-ideal geometries and experimental constraints, higher order multipole fields get superposed on the predominantly linear field. This results in the equations of motion taking the form of (weakly) nonlinear and coupled Mathieu equations. In this paper, however, we consider a single, weakly nonlinear Mathieu equation.

The main problem in studying ion behavior in the neighborhood of the Mathieu stability boundary is that it is not possible to derive a closed form solution for ion motion when field inhomogeneities are present. Sudakov [22] has presented an insightful analysis of the slow variation in amplitude of the ion motion, which he calls the "beat" envelope, near the stability boundary. He showed that in case of positive octopole superposition, there exists an effective potential well in the stable region. The width and depth of this well decreases as q_z approaches the stability boundary. In case of negative octopole superposition and hexapole superposition of either sign, the existence of a double well potential in the unstable region of the Mathieu stability plot causes delayed ejection of ions from the trap.

In this paper we present a detailed and systematic analytical study of ion ejection near the nominal stability boundary ($q_z^* = 0.908046$) for practical Paul traps. We go beyond the work of Sudakov [22] in three ways. First, we adopt a formal perturbation method, the method of multiple scales (MMS), which has enabled us to proceed up to the fourth order (Appendix A). This may be useful when the weights of multipole superpositions are relatively larger. However, we use only the second order slow flow for obtaining the phase portraits in this paper, since we have assumed weak multipole superpositions. Secondly, we have incorporated higher order multipoles (hexapole, octopole, decapole and dodecapole superpositions) in the governing equation. With this, we obtain new insights into the dynamics associated with these multipole superpositions within the trapping field. Finally, we use phase portraits to provide an alternative view of the slow modulation dynamics as the ions approach the stability boundary, to understand early and delayed ejection of ions. Our results match Sudakov [22] up to second order, except for an apparent error in one of his terms, which we have corrected.

As a technical matter, we mention that the application of the MMS at the stability boundary involves somewhat greater complications than the application of the MMS, or the related method of averaging [23], to resonant points inside the nominal stability region because in the latter case the unperturbed equation has two linearly independent periodic solutions.

2. Equation of motion

In the literature, the potential distribution inside a trap with field inhomogeneities in terms of spherical coordinates (ρ, θ, φ) is given by [24]

$$\phi(\rho, \theta, \varphi) = \phi_0 \sum_{n=0}^{\infty} A_n \frac{\rho^n}{r_0^n} P_n(\cos\,\theta), \tag{2}$$

where P_n is the Legendre polynomial of order n, A_n the dimensionless weight factor for the n^{th} multipole term, ρ the radial position and r_0 is chosen to be the radius of the central ring electrode in our study. ϕ_0 is given by

$$\phi_0 = U + V\,\cos\,\Omega t, \tag{3}$$

where U is the applied d.c. potential, and V is the amplitude of the applied rf potential. In this study we consider four higher order multipoles which include A_3, A_4, A_5 and A_6, corresponding to hexapole, octopole, decapole and dodecapole, respectively, in Eq. (2). We use the notation and sign convention of Beaty [24] for representing the higher order multipoles. Since our focus is on axial (z) instability, we set $r \equiv 0$. Following the procedure adopted by Sevugarajan and Menon [25] and Abraham et al.

[26], the uncoupled equation of motion of trapped ions in the axial (z) direction in an experimental trap reduces to a nonlinear Mathieu equation:

$$\frac{\mathrm{d}^2x}{\mathrm{d}\tau^2} + (a_z + 2q_z\,\cos\,2\tau) \times \left(x + \frac{3h}{2}x^2 + 2fx^3 + \frac{5d}{2}x^4 + 3kx^5\right) = 0, \quad (4)$$

where $x = z/r_0$ is the axial position of the ion normalized with respect to r_0, $\tau = \Omega t/2$, and $h(= A_3/A_2)$, $f(= A_4/A_2)$, $d(= A_5/A_2)$ and $k(= A_6/A_2)$ are the proportion of hexapole, octopole, decapole and dodecapole nonlinearity, respectively, to the quadrupole superposition, A_2. Also, a_z and q_z are Mathieu parameters for the nonlinear trap and are given by

$$a_z = \frac{8eA_2U}{mr_0^2\Omega^2}; \qquad q_z = \frac{4eA_2V}{mr_0^2\Omega^2}, \quad (5)$$

where e/m is the charge to mass ratio of the ion.

A point that needs mention is related to the usage of the descriptors "positive" and "negative" for multipole superpositions. In the mass spectrometry literature, the sign is implicitly attributed to the specific multipole by assuming that the sign of the quadrupole superposition is positive. In actual practice, when the end cap electrodes of the ion trap are grounded as is usually done in mass selective boundary ejection experiments, the weight of the quadrupole superposition, A_2 is negative. Consequently, "positive" multipole superposition implies that A_n and A_2 have the same sign and "negative" multipole superposition implies A_n and A_2 have opposite signs.

In mass selective ejection experiments, where only the rf voltage is applied, the equation of motion (Eq. (4)) takes the form:

$$\frac{\mathrm{d}^2x}{\mathrm{d}\tau^2} + 2q_z\,\cos\,2\tau\left(x + \frac{3h}{2}x^2 + 2fx^3 + \frac{5d}{2}x^4 + 3kx^5\right) = 0, \quad (6)$$

since a_z is set to 0. Ion destabilization occurs at the stability boundary (corresponding to $\beta_z = 1$, where β_z is related to the Mathieu parameters a_z and q_z) in the Mathieu stability plot [27]. In our discussion the q_z value at the nominal point of destabilization in ideal traps will be referred to as q_z^*, which happens to be 0.908046, as shown below.

In the method of multiple scales adopted here, we need to order the nonlinearities. The following ordering scheme has been adopted:

$$h = \frac{2\sqrt{\epsilon}\bar{h}}{3}, \qquad f = \frac{\epsilon\bar{f}}{2}, \qquad d = \frac{2\sqrt{\epsilon}\bar{d}}{5}, \qquad k = \frac{\epsilon\bar{k}}{3}, \quad (7)$$

where $\bar{h}$, $\bar{f}$, $\bar{d}$, $\bar{k}$ and ϵ will determine the strengths of the nonlinearities. Note that all even superpositions have been ordered as ϵ and odd superpositions as $\sqrt{\epsilon}$. Moreover, $\bar{h}$, $\bar{f}$, $\bar{d}$ and $\bar{k}$ are of $\mathcal{O}(1)$, with the "smallness" of these terms governed by $0 < \epsilon \ll 1$. Further, to study the dynamics near q_z^*, we introduce a detuning parameter Δ and write

$$q_z = q_z^* + \epsilon\Delta. \quad (8)$$

Thus by assigning negative and positive values to Δ, we can study the dynamics associated with early and delayed ejection, respectively.

Substituting Eqs. (7) and (8) into Eq. (6), the governing equation of our system takes the form:

$$\frac{\mathrm{d}^2x}{\mathrm{d}\tau^2} + 2(q_z^* + \epsilon\Delta) \times \cos\,2\tau\left(x + \sqrt{\epsilon}\bar{h}x^2 + \epsilon\bar{f}x^3 + \sqrt{\epsilon}\bar{d}x^4 + \epsilon\bar{k}x^5\right) = 0. \quad (9)$$

3. Analysis using multiple scales

In the method of multiple scales [28–31], we assume that the solution to the original equation can be represented as a function of multiple time scales. Here, we choose $T_0 = \tau$, $T_1 = \sqrt{\epsilon}\tau$, $T_2 = \epsilon\tau$, ... T_0 is the fast (usual) time and T_1, T_2, ... are the slow times. This particular choice is justified in Appendix B. The solution $x(\tau)$ to Eq. (9) is sought in the form:

$$x(\tau) = X(T_0, T_1, T_2, \ldots). \quad (10)$$

Further, X is expanded as

$$X(T_0, T_1, T_2, \ldots) = X_0(T_0, T_1, T_2, \ldots) + \sqrt{\epsilon}X_1(T_0, T_1, T_2, \ldots) + \epsilon X_2(T_0, T_1, T_2, \ldots) + \epsilon\sqrt{\epsilon}X_3(T_0, T_1, T_2, \ldots) + \mathcal{O}(\epsilon^2). \quad (11)$$

The derivatives with respect to τ are:

$$\frac{\mathrm{d}(.)}{\mathrm{d}\tau} = \frac{\partial(.)}{\partial T_0} + \sqrt{\epsilon}\frac{\partial(.)}{\partial T_1} + \epsilon\frac{\partial(.)}{\partial T_2} + \mathcal{O}(\epsilon\sqrt{\epsilon}), \quad (12)$$

$$\frac{\mathrm{d}^2(.)}{\mathrm{d}\tau^2} = \frac{\partial^2(.)}{\partial T_0^2} + 2\sqrt{\epsilon}\frac{\partial^2(.)}{\partial T_0\partial T_1} + \epsilon\left(\frac{\partial^2(.)}{\partial T_1^2} + 2\frac{\partial^2(.)}{\partial T_0\partial T_2}\right) + \mathcal{O}(\epsilon\sqrt{\epsilon}). \quad (13)$$

Substituting Eqs. (11) through (13) in Eq. (9), expanding and collecting terms using a symbolic algebra package (MAPLE), we obtain:

$$\frac{\partial^2X_0}{\partial T_0^2} + 2q_z^*\,\cos(2T_0)X_0 + \sqrt{\epsilon}\left[\frac{\partial^2X_1}{\partial T_0^2} + 2q_z^*\,\cos(2T_0)\left(X_1 + \bar{h}X_0^2 + \bar{d}X_0^4\right) + 2\frac{\partial^2X_0}{\partial T_0\partial T_1}\right] + \epsilon\left[\frac{\partial^2X_2}{\partial T_0^2} + \frac{\partial^2X_0}{\partial T_1^2} + 2\frac{\partial^2X_0}{\partial T_0\partial T_2} + 2\frac{\partial^2X_1}{\partial T_0\partial T_1} + 2\,\cos(2T_0)\left(q_z^*X_2 + 2q_z^*\bar{h}X_0X_1 + q_z^*\bar{f}X_0^3 + 2q_z^*\bar{d}X_0^3X_1 + q_z^*\bar{k}X_0^5 + \Delta X_0\right)\right] + \mathcal{O}(\epsilon\sqrt{\epsilon}) = 0. \quad (14)$$

Table 1
Values of a_k's and b_k's

k	a_k	b_k
0	1.00000000...	−1.13521939...
1	0.10126539...	−0.18286643...
2	0.00368062...	−0.00812047...
3	0.00006822...	−0.00017002...
4	0.00000076...	−0.00000208...
5	$0.57401517 \times 10^{-8}$	$-0.16624533 \times 10^{-7}$
6	$0.30842821 \times 10^{-10}$	$-0.94071713 \times 10^{-10}$

As is usual for the MMS, we will solve the above sequentially for different orders (powers of ϵ). Indeterminacy in the solution at each stage, as usual, will be eliminated by insisting on a bounded solution at the next stage (a process called removal of secular terms). However, the form of the secular terms, and our process of identifying them, is somewhat unusual and described in detail below. Note that, for our higher order calculations, we retained more terms in the above expansion, these are not presented here for the sake of brevity.

3.1. Solution at $\mathcal{O}(1)$

From Eq. (14) at $\mathcal{O}(1)$, we have the linear Mathieu equation:

$$\frac{\partial^2 X_0}{\partial T_0^2} + 2q_z^* \cos(2T_0)X_0 = 0. \tag{15}$$

Since this equation corresponds to the ion motion at the boundary ($q_z = q_z^*$), the solution consists of a 2π-periodic function and a linearly growing function [32].

Let the periodic function be ξ_1. It can be written as a cosine series given by

$$\xi_1 = \sum_{k=0}^{M} a_k \cos((2k+1)T_0), \tag{16}$$

where $M = \infty$ for the exact solution, but we will truncate the series at a suitably large value of M. In our computation, we set $M = 12$.

To obtain (or rather, verify) the numerical value of q_z^*, we substitute the truncated cosine series into Eq. (15). Collecting the coefficients of the harmonics retained in the approximation (Eq. (16)) and equating them to 0, we get $M+1$ simultaneous linear equations in unknown a_k's. For nontrivial solutions to exist, the determinant of the coefficient matrix, which is a polynomial in q_z^*, must be 0. When this equation is solved, the smallest root gives $q_z^* = 0.908046$. In what follows, we take[1] $q_z^* = 0.908046$.

In order to obtain the a_k's (and thus ξ_1), we substitute $q_z^* = 0.908046$ into the $M+1$ linear equations obtained earlier. Since the $M+1$ equations are linearly dependent, we choose $a_0 = 1$ for convenience, drop the equation corresponding to the coefficient of cos T_0, and use the remaining M equations to find the remaining a_k's (see Table 1).

[1] More digits were retained in our calculations using MAPLE. For verification by interested readers, $q_z^* = 0.9080463337\ldots$

The linearly growing part of the solution of Eq. (15) has the form $\xi_2 + T_0\,\xi_1$ [32], where ξ_2 is 2π-periodic. When this form is inserted into Eq. (15), we get the differential equation for ξ_2 as

$$\ddot{\xi}_2 + 2q_z^* \cos(2T_0)\xi_2 = -2\dot{\xi}_1. \tag{17}$$

ξ_2 can be approximated by a truncated Fourier series as

$$\xi_2 = \sum_{k=0}^{M} b_k \sin((2k+1)T_0), \tag{18}$$

where, again, we use $M = 12$. Substituting this into the differential equation for ξ_2 and collecting terms, we get $M+1$ linear simultaneous equations which can be directly solved to obtain the b_k's (Table 1). The a_k's and b_k's progressively decrease in magnitude and their numerical values for $k > 6$ are not presented here, although $M = 12$ and many digits of precision were used in our MAPLE calculation. It is clear that choosing $M = 12$ is more than enough for practical purposes.

The general solution to Eq. (15) can then be written as

$$X_0 = A(T_1, T_2)\xi_1(T_0) + B(T_1, T_2)(\xi_2(T_0) + T_0\xi_1(T_0)), \tag{19}$$

where A and B are arbitrary functions of T_1 and T_2.

We now set $B \equiv 0$ which eliminates the rapidly growing part in Eq. (19). This may initially seem somewhat arbitrary. Note, however, that by choosing $B \equiv 0$, we can obtain one solution and numerics will show that the solution so obtained is useful. For a similar example of setting the coefficient of a rapidly increasing term to 0 and some relevant discussion, see Chatterjee and Chatterjee [33]. Thus the solution to the $\mathcal{O}(1)$ equation is taken as

$$X_0 = A(T_1, T_2)\xi_1(T_0). \tag{20}$$

It may be noted that ξ_2 does not appear in X_0 in Eq. (20). However, ξ_2 will be required in the subsequent analysis.

3.2. Solution at $\mathcal{O}(\sqrt{\epsilon})$

Before we go to $\mathcal{O}(\sqrt{\epsilon})$, consider:

$$\ddot{x} + P(t)\dot{x} + Q(t)x = R(t), \tag{21}$$

where $P(t)$, $Q(t)$, $R(t)$ are bounded, periodic functions with period T. Assume that the complementary solution to Eq. (21) is a linear combination of h_1 and $h_2 + \alpha\, t\, h_1$ where h_1 and h_2 are T-periodic and α is some nonzero constant. Das and Chatterjee [34] show that secular terms in the solution to Eq. (21) do not grow in amplitude faster than t^2. Moreover, under arbitrary but periodic forcing, secular terms in the particular solution are a linear combination of $t(2h_2 + \alpha\, t h_1)$ and th_1. We will use these results below.

We now return to Eq. (14) at $\mathcal{O}(\sqrt{\epsilon})$, and we have:

$$\frac{\partial^2 X_1}{\partial T_0^2} + 2\,q_z^* \cos(2T_0)X_1 = -2\frac{\partial^2 X_0}{\partial T_0 \partial T_1} - 2\,q_z^* \cos(2T_0)\,(\bar{h}X_0^2 + \bar{d}X_0^4). \tag{22}$$

We note the similarity between Eqs. (22) and (21) by identifying:

$$x \equiv X_1, \qquad P(t) \equiv 0, \qquad Q(t) \equiv 2q_z^* \cos(2T_0),$$

$$R(t) \equiv -2\frac{\partial^2 X_0}{\partial T_0 \partial T_1} - 2\,q_z^* \cos(2T_0)\,(\bar{h}X_0^2 + \bar{d}X_0^4).$$

The complementary solution to Eq. (22) is a linear combination of ξ_1 and $\xi_2 + T_0\,\xi_1$ where ξ_1 and ξ_2 are given by Eqs. (16) and (18) and are 2π-periodic. Therefore, secular terms in the particular solution are a linear combination of $T_0\,(2\xi_2 + T_0\,\xi_1)$ ($\alpha = 1$ in our case) and $T_0\,\xi_1$. The general solution to Eq. (22) can be written as [34]

$$X_1 = c_1\xi_1 + c_2(\xi_2 + T_0\xi_1) + c_3 T_0\,\xi_1 + c_4 T_0\,(2\xi_2 + T_0\,\xi_1) + \Psi(T_0), \tag{23}$$

where c_1 through c_4 are constants and Ψ is 2π-periodic in T_0. Moreover, c_1 and c_2 are arbitrary, being part of the complementary solution. One linearly growing part of the particular solution can be nullified by a linearly growing part of the complementary solution (by choosing $c_2 = -c_3$). Although c_2 is thereby fixed, c_1 is still arbitrary. We now choose c_1 such that it nullifies the coefficient of $\cos\,T_0$ in $\Psi(T_0)$. By these arguments and simplifications:

$$X_1 = c_4 T_0\,(2\,\xi_2 + T_0\,\xi_1) + \Psi(T_0), \tag{24}$$

where $\Psi(T_0)$ is 2π-periodic, has absorbed $c_1\,\xi_1 - c_3\,\xi_2$ and has no $\cos\,T_0$ term, i.e.,

$$X_1 = C_{2N+1} + \sum_{k=2}^{N} C_k\,\cos(kT_0) + \sum_{k=1}^{N} C_{k+N}\sin(kT_0) + C_{2N+2}\,T_0\,(2\xi_2 + T_0\xi_1), \tag{25}$$

where N is some positive integer (here we have taken $N = 12$) and the C_k's are coefficients to be determined. Note that $\cos\,T_0$ has been left out above.

Since ξ_1 and ξ_2 are approximate and the periodic part of X_1 is also approximate, the form of X_1 satisfies Eq. (22) only approximately. Therefore, after substituting Eqs. (25) into (22), the left hand side will not be exactly equal to the right hand side. Bringing all terms to the left hand side, we obtain a nonzero residual. The unknown C_k's are determined by carrying out the Galerkin projection procedure used in a related context by Das and Chatterjee [34]. In this procedure the residual is separately multiplied by each basis function in the assumed form of the general solution (right hand side of Eq. (25)), namely

$$1,\ T_0\,(2\xi_2 + T_0\xi_1),\ \sin\,T_0,\ \sin(2T_0),\ \cos(2T_0),\ \ldots,$$

and then each such product is integrated over one period (from 0 to 2π). Setting the integrals thus obtained to 0, we obtain $2N + 1$ linear equations in the unknown coefficients C_k's. We solve for these coefficients and substitute them in Eq. (25) to obtain X_1.

A key point is that coefficient C_{2N+2} must be set to 0 to avoid the secular terms and this, as is usual in the MMS, enables us to obtain the slow flow. From MAPLE we obtain, at $\mathcal{O}(\sqrt{\epsilon})$:

$$C_{2N+2} = 0.12873832 \times 10^{-9}\,\bar{h}\,A^2 - 0.30186541 \times 10^{-7}\,\bar{d}\,A^4 - 0.39256924 \times 10^{-9}\,\frac{\partial A}{\partial T_1}. \tag{26}$$

We note that the numerical coefficients are very small. We need to determine if they are actually numerically corrupted versions of exactly 0, i.e., if they should be set to 0. Noting that, from the Galerkin procedure, we have simultaneously obtained:

$$C_2 = -0.67189535\,\bar{d}\,A^4 - 0.60163836\,\bar{h}\,A^2, \tag{27}$$

and

$$C_4 = 0.0045506\,\bar{d}\,A^4 - 0.006558\,\bar{h}\,A^2, \tag{28}$$

which involve much larger numerical coefficients, we conclude that C_{2N+2} is actually 0. Thus, we take $C_{2N+2} = 0$, and obtain no useful information at this order. We must proceed to a higher order calculation.

There are some technical issues in doing such higher order calculations, regarding the asymptotic validity of the method, but good approximations will nevertheless be obtained. The technical issues related to asymptotic validity are identical to those discussed in Nandakumar and Chatterjee [35] for averaging, and are not discussed here. The solution X_1 is given in Appendix C.

3.3. Solution at $\mathcal{O}(\epsilon)$

We now proceed to $\mathcal{O}(\epsilon)$ which will provide useful information about the evolution of the amplitude A of the solution. From Eq. (14), at $\mathcal{O}(\epsilon)$, we have

$$\frac{\partial^2 X_2}{\partial T_0^2} + 2\,q_z^*\cos(2T_0)X_2 = -\frac{\partial^2 X_0}{\partial T_1^2} - 2\frac{\partial^2 X_0}{\partial T_0 \partial T_2} - 2\frac{\partial^2 X_1}{\partial T_0 \partial T_1} - 2\cos(2T_0)X_0 - 2\cos(2T_0) \times q_z^*\,(2\bar{h}\,X_0X_1 + \bar{f}\,X_0^3 + 2q_z^*\bar{d}X_0^3X_1 + q_z^*\bar{k}X_0^5). \tag{29}$$

Eq. (29) also fits the form of Eq. (21). As was done for X_1 at $\mathcal{O}(\sqrt{\epsilon})$, here we take

$$X_2 = D_{2N+1} + \sum_{k=2}^{N} D_k\,\cos(kT_0) + \sum_{k=1}^{N} D_{k+N}\sin(kT_0) + D_{2N+2}\,T_0\,(2\xi_2 + T_0\xi_1), \tag{30}$$

where $N = 12$ as earlier, and D_k's are coefficients to be determined. We follow the Galerkin projection procedure again (as described earlier) to solve for the unknown D_k's. Setting D_{2N+2} equal to 0, we obtain:

$$-1.9438\bar{h}^2A^3 + 0.44483\,\bar{f}\,A^3 - 4.7213\bar{d}^2A^7 + 0.48561\bar{k}A^5 - 6.4286\bar{h}\bar{d}A^5 + 0.43865\Delta A - 0.50000\frac{\partial^2 A}{\partial {T_1}^2} = 0. \tag{31}$$

From Eq. (13), we have

$$\ddot{A} = \frac{\mathrm{d}^2 A}{\mathrm{d}\tau^2} = \frac{\partial^2 A}{\partial T_0^2} + 2\sqrt{\epsilon}\frac{\partial^2 A}{\partial T_0 \partial T_1} + \epsilon\left(\frac{\partial^2 A}{\partial T_1^2} + 2\frac{\partial^2 A}{\partial T_0 \partial T_2}\right) + \mathcal{O}(\epsilon\sqrt{\epsilon}). \quad (32)$$

Since amplitude A is not a function of the fast variable T_0, we have

$$\ddot{A} = \epsilon\frac{\partial^2 A}{\partial T_1^2} + \mathcal{O}(\epsilon\sqrt{\epsilon}), \quad (33)$$

giving the required slow flow as

$$\ddot{A} = \epsilon(0.8773\Delta A - 3.8877\bar{h}^2 A^3 + 0.8897\bar{f}A^3 - 12.8564\bar{h}\bar{d}A^5 + 0.9712\bar{k}A^5 - 9.4429\bar{d}^2 A^7) + \mathcal{O}(\epsilon\sqrt{\epsilon}). \quad (34)$$

Note that, after setting $D_{2N+2} = 0$, we also have X_2. The solution X_2 is provided in Appendix C and is needed for higher order calculations.

Eq. (34) is the second order slow flow for ion motion in the presence of hexapole, octopole, decapole and dodecapole superpositions. The presence of ϵ and Δ in the equation enables us to visualize ion dynamics at different values of detuning from q_z^*. In order to compare these results with the beat envelope equations of Sudakov [22] (where separate equations were presented for hexapole and octopole superpositions), we plot the time trajectories predicted by these equations. To do this we transform the coefficients of Eq. (34) to the form of the beat envelope equations. Details of this comparative study are presented in Appendix D, where agreement is observed with Sudakov's results except for one erroneous numerical coefficient which we correct here.

Using this systematic approach we have actually carried out calculations up to the fourth order, and the final fourth order slow flow equation is given, for completeness, in Appendix A (details are available in Marathe (2006)).[2] This equation may be of use in the presence of somewhat larger weights of multipole superpositions. However, in the present study, we will use only the second order slow flow (Eq. (34)) for generating relevant phase portraits below.

3.4. Numerical verification

We next check the correctness of the slow flow we have obtained. We do this by first integrating Eq. (9) numerically, using the built-in routine ODE45 from MATLAB, with some chosen initial conditions. Numerical tolerances of 10^{-8} are specified for the integration routine. Figs. 1–3 show comparisons between numerically obtained solutions of Eq. (9) and the amplitude obtained by solving the slow flow (Eq. (34)). In these plots we have selected $\epsilon = 0.001$, and the initial conditions for integration of Eq. (9) were taken as $x(0) = 0.01$ and $\dot{x}(0) = 0$. We obtain the corresponding initial conditions for the slow flow (Eq. (34)) by a method described in Appendix E. The values of parameters used are given in the respective figure captions. For the purpose of comparison of the two equations for a specific nonlinearity, the weights of the other superpositions are set to 0 in both Eqs. (9) and (34).

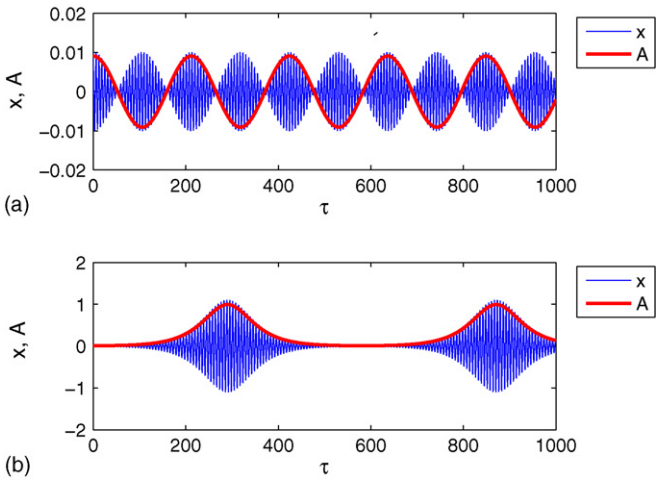

Fig. 1. Comparison of amplitude (A) determined by solving the slow flow with the original Mathieu equation (x) for positive and negative octopole. In both plots, $\epsilon = 0.001$, $x(0) = 0.01$, $\dot{x}(0) = 0$, $A(0) = 0.0091$, $\dot{A}(0) = 0$ and $\bar{h} = \bar{d} = \bar{k} = 0$. Further, we use for (a) $\bar{f} = 1$, $\Delta = -1$; for (b) $\bar{f} = -1$, $\Delta = 1$.

Fig. 1(a) presents the results for positive octopole and Fig. 1(b) for negative octopole. From the figure, a good match can be seen between the full numerical solution and MMS approximation. Fig. 2(a) and (b) show results for hexapole and decapole superpositions where the effect of nonlinearity is sign independent. Fig. 3(a) shows the comparison for positive dodecapole while Fig. 3(b) is for negative dodecapole. From these plots, it can be observed that the slow flow adequately represents the slow temporal variation in amplitude of the system in the neighborhood of the stability boundary.

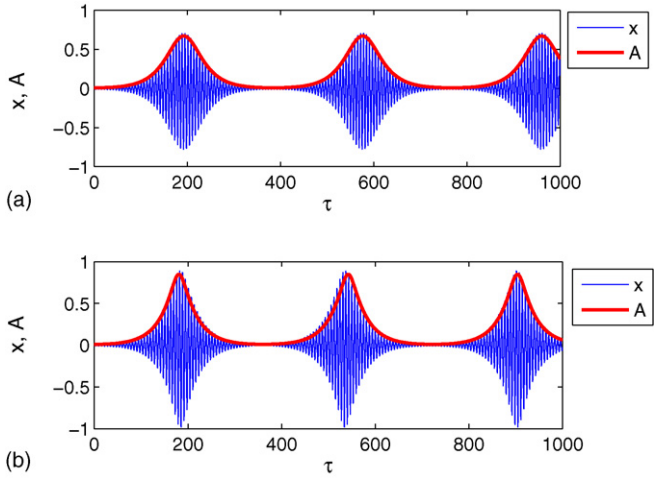

Fig. 2. Comparison of amplitude (A) determined by solving the slow flow with the original Mathieu equation (x) for hexapole and decapole. In both plots, $\epsilon = 0.001$, $\Delta = 1$, $x(0) = 0.01$, $\dot{x}(0) = 0$ and $\bar{f} = \bar{k} = 0$. Further, we use for (a) $\bar{h} = 1$, $\bar{d} = 0$, $A(0) = 0.0091$, $\dot{A}(0) = 0$; for (b) $\bar{d} = 1$, $\bar{h} = 0$, $A(0) = 0.0101$, $\dot{A}(0) = 0$.

[2] A. Marathe, PhD Thesis, Indian Institute of Science, in preparation.

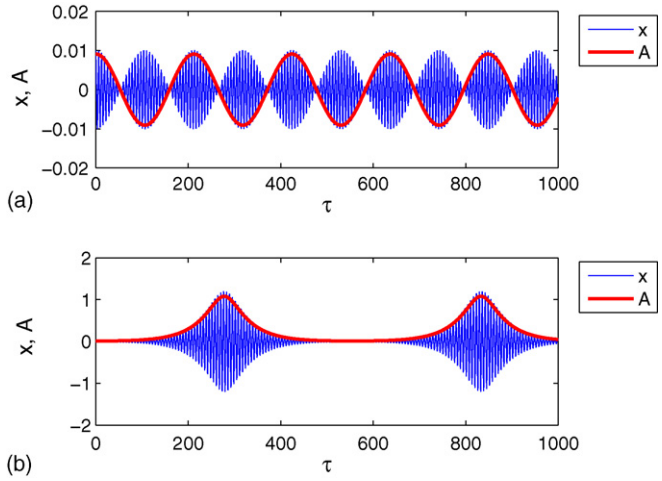

Fig. 3. Comparison of amplitude (A) determined by solving the slow flow with the original Mathieu equation (x) for positive and negative dodecapole. In both plots, $\epsilon = 0.001$, $x(0) = 0.01$, $\dot{x}(0) = 0$, $A(0) = 0.0091$, $\dot{A}(0) = 0$ and $\bar{h} = \bar{f} = \bar{d} = 0$. Further, we use for (a) $\bar{k} = 1$, $\Delta = -1$; for (b) $\bar{k} = -1$, $\Delta = 1$.

4. Results and discussion

Eq. (34) is the second order slow flow which describes variation in amplitude of ion motion in the presence of hexapole, octopole, decapole and dodecapole multipole superpositions. While the octopole ($\bar{f}$) and decapole ($\bar{k}$) appear as linear terms, the hexapole ($\bar{h}$) and decapole ($\bar{d}$) appear independently as quadratic terms as well as in combination in one of the terms. This last observation, namely that of $\bar{h}$ and $\bar{d}$ appearing as a combination, has two interesting consequences. First, the sign of the hexapole will affect dynamics only if decapole superposition is also present. Second, for the sign of hexapole superposition to affect ion dynamics its sign change must be independent of decapole superposition. These consequences are also borne out by the fourth order slow flow which includes a larger number of terms (see Appendix A and the caveats therein).

We now return to our original problem of understanding ion dynamics in the presence of field inhomogeneities. The nonlinearities considered here are hexapole, octopole, decapole and dodecapole. This study will rely on interpreting numerically generated phase portraits, obtained from the slow flow (Eq. (34)), at different values of Δ. In the phase portraits presented, we have varied Δ from -2 to $+8$, and the corresponding q_z values are presented in Table 2 for ready reference. These q_z values are calculated by substituting $q_z^* = 0.908046$ and $\epsilon = 0.001$ in Eq. (8). All the phase portraits are generated keeping the value of ϵ at 0.001. The slow flow equations are integrated repeatedly for a large number of initial conditions and the phase portraits are obtained by plotting the derivative of the amplitude ($\dot{A}$) on the y-axis and amplitude (A) on the x-axis.

Although in real traps the field has more than one higher order multipole superposition, for the sake of clarity of the discussion we study the effect of each multipole superposition individually. The effect of combinations of multipoles may be evaluated by a suitable choice of terms in the slow flow equation (Eq. (34)) and will not be explicitly discussed in this paper.

Table 2
q_z at different values of Δ, for $\epsilon = 0.001$

Δ	q_z
−2.0	0.9060463
−1.0	0.9070463
−0.5	0.9075463
−0.1	0.9079463
−0.001	0.9080453
0.25	0.9082963
0.6	0.9086463
1.0	0.9090463
2.0	0.9100463
8.0	0.9160463

4.1. Positive octopole

We set $\bar{h} = \bar{d} = \bar{k} = 0$ in Eq. (34) to study the effect of octopole superpositions. The right hand side of Eq. (34) is a cubic polynomial in amplitude A. The roots of this polynomial are

$$(-0.9940\sqrt{-\Delta/\bar{f}}, 0), \quad (0, 0) \quad \text{and} \quad (0.9940\sqrt{-\Delta/\bar{f}}, 0).$$

These, if real, are also the fixed points of the slow flow. Since $\bar{f}$ is positive, for positive values of Δ, there exists only one fixed point at (0,0) and this is a saddle, indicating that the ion is unstable. For negative Δ values, however, there are three fixed points. For instance, for $f = 0.01$ (i.e., $\bar{f} = 20$ for $\epsilon = 0.001$) and $\Delta = -2$, these fixed points occur at $A = 0$, $A = \pm 0.3143$. The two nonzero fixed points are now saddles and consequently ions will be stable only near the origin (a center) where the solution is bounded. As we vary Δ from -2 towards 0 (that is, towards the stability boundary), the nonzero fixed points move towards each other. This can be observed from Fig. 4(a)–(d) which show the phase portraits generated by numerically integrating Eq. (34). For $\Delta = -0.5$, -0.1, and -0.001, the nonzero fixed points are ± 0.1572, ± 0.0703, and ± 0.00703, respectively.

From Fig. 4(a)–(d), it can also be observed that the area of the region around the center where the solution is bounded diminishes as Δ is varied from -2 to -0.001, and ions with initial

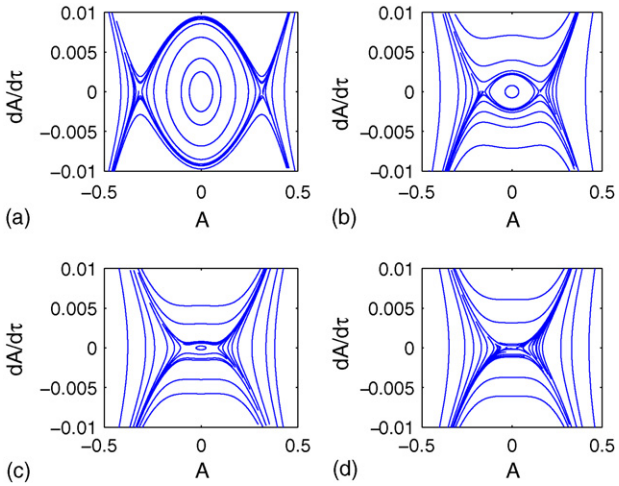

Fig. 4. Phase portrait for 1% octopole ($f = 0.01$, $\bar{f} = 20$, $\epsilon = 0.001$) for Δ values of (a) -2, (b) -0.5, (c) -0.1 and (d) -0.001.

conditions which would earlier have been stable now are unstable and escape to infinity. For Δ values very close to 0, but less than 0, the area in the phase space where the solution is bounded is so small that all ions with significant energies escape. The phase portraits present qualitatively a similar picture to Sudakov's [22] observation that for positive octopole there is a potential well within the stable region and the width and depth of this well decreases as q_z approaches the boundary. In the context of our study, the central region in the phase portrait (with closed curves) corresponds to the potential well discussed by Sudakov [22].

4.2. Negative octopole

We now consider the ion dynamics in the neighborhood of the stability boundary with 1% negative octopole nonlinearity. Since $\bar{f}$ is negative, for negative values of Δ, Eq. (34) will have only one fixed point. This will be a center and hence the ion will be stable. For positive values of Δ (i.e., beyond the nominal stability boundary), there exist three fixed points consisting of a saddle and two centers (one on each side of the saddle). As Δ is increased to values greater than 0, these centers move away from each other. The centers for $\Delta = 2$ are at $A = \pm 0.3143$ and for $\Delta = 8$ are at $A = \pm 0.6287$.

Fig. 5(a)–(d) shows the phase portraits generated by numerically integrating Eq. (34) for Δ values corresponding to -1, 0, 2 and 8, respectively, for 1% negative octopole nonlinearity. Referring to Fig. 5(a) and (b), there exists only one fixed point and this is a center. All ions which were originally located near the trap center will continue to execute stable oscillations and will not escape from the trap. When the q_z value of the ion is increased beyond q_z^* (where Δ is positive), the phase portrait qualitatively changes its nature. As can be seen from Fig. 5(c) and (d), the origin which was earlier a center now becomes a saddle and two new centers are created. Thus an ion will oscillate in a path (in averaged or slow phase space) that encircle either one of the centers, or both centers. For very small positive values of Δ, ion amplitude does not exceed the trap boundary and ions are therefore confined within the trap cavity. Increasing the detuning parameter Δ increases the maximum amplitude that an ion oscillation encircling a center can have. Eventually, for large enough Δ, ion motion amplitudes exceed the trap dimensions, and so the ion gets ejected (also see numerical simulation of this phenomenon in Sudakov [22]). Thus, in the presence of negative octopole superposition, ion oscillations continue to be inherently stable well beyond q_z^* and ion escapes from the trap only when amplitude reaches the trap boundary.

Here too, our results are consistent with Sudakov's [22] observation of a double well potential function for negative octopole superposition. The regions around the two centers (with closed curves) on either side of the saddle, observed for positive values of Δ, correspond to the double well potential shown in that study.

4.3. Hexapole

The effect of hexapole superposition can be studied by setting $\bar{f} = \bar{d} = \bar{k} = 0$ in Eq. (34). It is observed that the hexapole nonlinearity parameter $\bar{h}$ appears in squared form which implies that the sign of hexapole nonlinearity will not affect the slow flow. This is in agreement with the simulation studies of Franzen et al. [36].

The roots of the polynomial obtained by equating the right hand side of Eq. (34) to 0 are:

$$(-0.4750\sqrt{\Delta/\bar{h}^2}, 0), \quad (0, 0) \quad \text{and} \quad (0.4750\sqrt{\Delta/\bar{h}^2}, 0).$$

For negative values of Δ there will be only one fixed point at (0, 0) and this will be a center. When Δ takes positive values, similar to the case of negative octopole nonlinearity, two centers and a saddle will appear.

Fig. 6(a)–(d) shows the phase portraits for 1% positive hexapole superposition (i.e., $\bar{h} = 0.47$ for $\epsilon = 0.001$) for Δ values -1, 0, 0.25 and 0.6, respectively. As can be seen from these figures, we get the same qualitative behavior as we obtained in case of the negative octopole nonlinearity, for both negative and positive values of Δ. This observation can also be

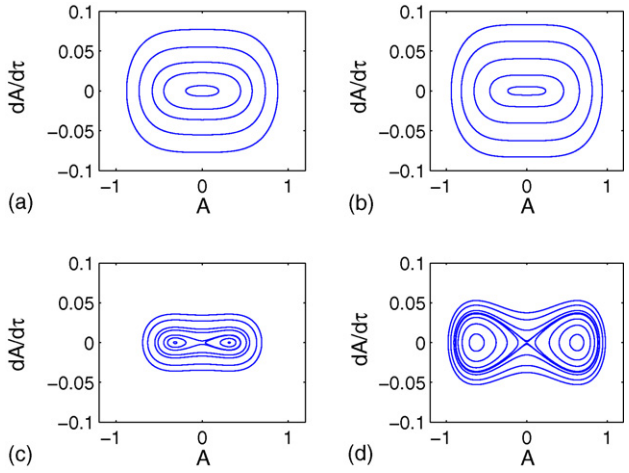

Fig. 5. Phase portrait for -1% octopole ($f = 0.01$, $\bar{f} = 20$, $\epsilon = 0.001$) for Δ values of (a) -1, (b) 0, (c) 2 and (d) 8.

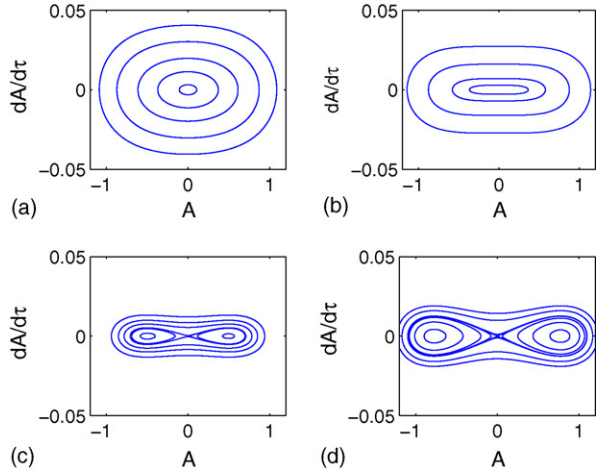

Fig. 6. Phase portrait for 1% hexapole ($h = 0.01$, $\bar{h} = 0.47$, $\epsilon = 0.001$) for Δ values of (a) -1, (b) 0, (c) 0.25 and (d) 0.6.

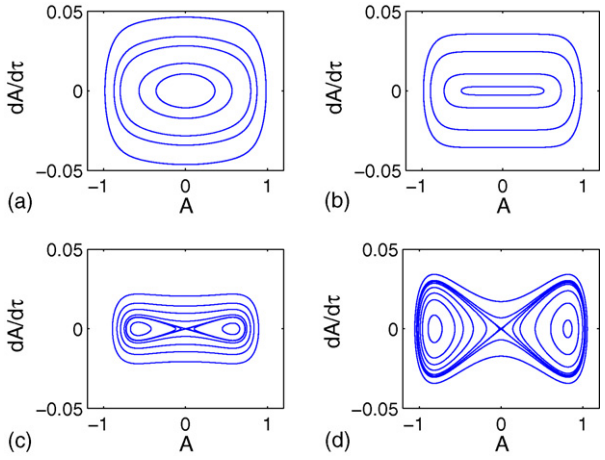

Fig. 7. Phase portrait for 1% decapole ($d = 0.01$, $\bar{d} = 0.79$, $\epsilon = 0.001$) for Δ values (a) −1, (b) 0, (c) 0.25 and (d) 2.

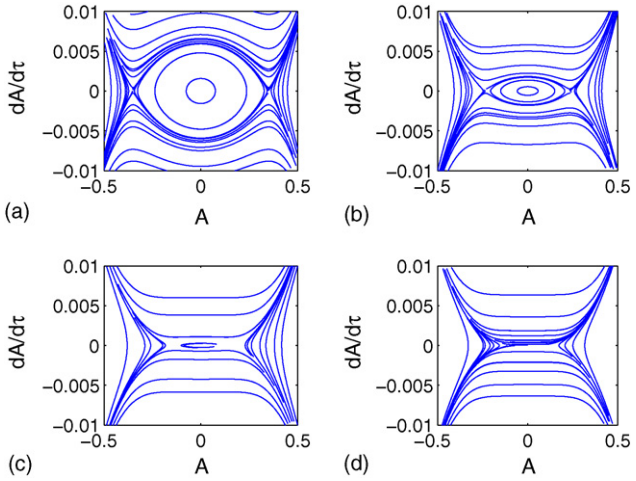

Fig. 8. Phase portrait for 1% dodecapole ($k = 0.01$, $\bar{k} = 30$, $\epsilon = 0.001$) for Δ values of (a) −0.5, (b) −0.1, (c) −0.01 and (d) −0.001.

understood from Eq. (34) where the qualitative behavior of the slow flow for the hexapole nonlinearity (in the absence of all others) will become similar to the slow flow for the negative octopole nonlinearity (in the absence of all others).

Notice, however that $\bar{h}\bar{d}$ appears in the slow flow, so sign independence is violated when multiple multipoles are present. Moreover, at the fourth order (see Appendix A) this symmetry is further lost due to the simultaneous presence of $\bar{h}\bar{d}$ as well as $\bar{h}^2\bar{d}$ (but see the caveats presented therein).

4.4. Decapole

To study the effect of decapole superposition we set $\bar{h} = \bar{f} = \bar{k} = 0$ in Eq. (34). The slow flow equation reduces to:

$$0.8773\Delta A - 9.4429\bar{d}^2 A^7 = 0. \tag{35}$$

Fig. 7(a)–(d) show the phase portraits for 1% decapole superposition (i.e., $\bar{d} = 0.79$ for $\epsilon = 0.001$). The phase portraits are qualitatively similar to the phase portraits obtained for hexapole superposition. As in the case of hexapole, delayed ejection is suggested by these phase portraits. The fixed point of the system when Δ is negative is (0,0). In this case the system exhibits stable oscillations. For positive values of Δ there will be three fixed points. For $\Delta = 0.25$ these are $(-0.5778, 0)$, $(0, 0)$ and $(0.5778, 0)$. From the phase portraits it can be observed that origin of the A–$\dot{A}$ plane is a saddle and the nonzero fixed points are centers. As Δ is increased to 2, the two nonzero fixed points move further apart to $(\pm 0.7857, 0)$. Ions are ejected from the trap when their amplitudes reach the trap boundary.

4.5. Positive dodecapole

The influence of dodecapole nonlinearity may be investigated by setting $\bar{h} = \bar{f} = \bar{d} = 0$ in Eq. (34). The slow flow reduces to

$$0.8773\Delta A - 0.9712\bar{k}A^5 = 0. \tag{36}$$

The system represented by this equation has three fixed points when Δ is negative and $\bar{k}$ is positive. The phase portraits for 1% dodecapole superposition (i.e., $\bar{k} = 30$ for $\epsilon = 0.001$) are shown in Fig. 8(a)–(d). When $\Delta = -0.5$ the fixed points are $(-0.3503, 0)$, $(0,0)$ and $(0.3503,0)$. The two nonzero fixed points are saddles and the origin is a center. As Δ is increased (that is, when q_z approaches q_z^*) the two nonzero fixed points move closer to the origin. From Fig. 8(d) corresponding to $\Delta = -0.001$, the center is almost gone and almost all initial conditions lead to unbounded solutions (ejection).

4.6. Negative dodecapole

When $\bar{k}$ is negative there exists only one fixed point at (0,0) for negative values of Δ. From Fig. 9(a), which is plotted for −1% dodecapole superposition at $\Delta = -1$, it can be seen that the system exhibits stable oscillations. However, for positive values of Δ there are three fixed points. Fig. 9(c) and (d) corresponding to $\Delta = 1$ and $\Delta = 8$, respectively, show that the nonzero fixed points are centers and the origin is a saddle. Ions are ejected from the trap when the ion oscillation amplitude reaches the trap boundary.

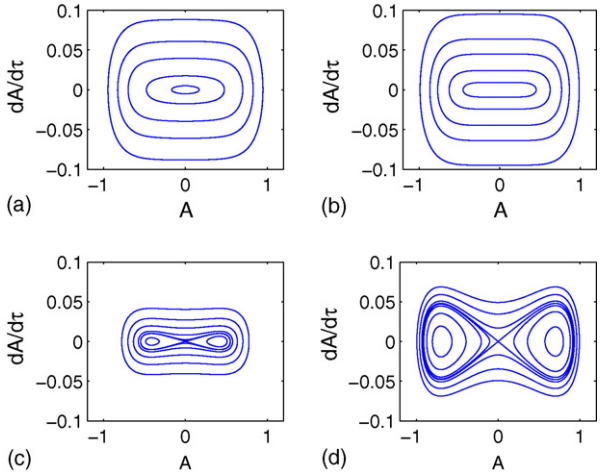

Fig. 9. Phase portrait for −1% dodecapole ($k = 0.01$, $\bar{k} = 30$, $\epsilon = 0.001$) for Δ values of (a) −1, (b) 0, (c) 1 and (d) 8.

5. Concluding remarks

The motivation of this paper was to understand the dynamics associated with early and delayed ejection of ions in Paul traps operated in the mass selective ejection mode. The studies reported in this paper will be of use in understanding dynamics at the stability boundary in all traps where the nonlinear Mathieu equation determines ion stability. Examples of mass analyzer configurations which are attracting considerable interest include the 2D (linear) Paul trap and the cylindrical trap, in addition to the hyperboloid geometry Paul trap.

The equation of motion of ions in the axial direction of the trap with hexapole, octopole, decapole and dodecapole superpositions was studied using the method of multiple scales. The ordering scheme used has allowed a systematic inclusion of higher order multipoles. Details of the analysis have been provided and our results are compared with those of Sudakov [22]. Although a fourth order slow flow equation has been computed and reported for potential future use in traps with larger weights of multipole superpositions, in our present study we have used the second order slow flow (Eq. (34)) for generating phase portraits.

$$\begin{aligned}\ddot{A} = \epsilon(&-12.8564\bar{h}\bar{d}A^5 - 9.44304\bar{d}^2A^7 - 3.88769\bar{h}^2A^3 + 0.97124\bar{k}A^5 + 0.87729\Delta A + 0.88965\bar{f}A^3 + 39.31546\bar{h}^2\dot{A}^2A \\ &- 5.50581\bar{f}\dot{A}^2A + 657.373\bar{d}^2\dot{A}^2A^5 - 20.2091\bar{k}\dot{A}^2A^3 + 411.774\bar{h}\bar{d}\dot{A}^2A^3) + \epsilon^2\,(-0.18369\Delta^2A - 125.986\bar{h}^4A^5 \\ &- 1892.91\bar{d}^4A^{13} + 290.186\bar{h}\bar{f}\bar{d}A^7 + 493.157\bar{h}\bar{d}\bar{k}A^9 + 389.577\bar{d}^2\bar{k}A^{11} - 1176.36\bar{h}^3\bar{d}A^7 - 3572.55\bar{h}^2\bar{d}^2A^9 \\ &+ 151.374\bar{h}^2\bar{k}A^7 - 7.64328\bar{d}\bar{k}A^7 + 23.3241\Delta\bar{h}^2A^3 + 78.6875\bar{h}^2\bar{d}A^5 + 251.73\bar{f}\bar{d}^2A^9 + 133.2125\Delta\bar{d}^2A^7 \\ &- 1.76775\Delta\bar{d}A^3 - 4394.78\bar{h}\bar{d}^3A^{11} - 3.843405\Delta\bar{k}A^5 + 121.976\Delta\bar{h}\bar{d}A^5 - 2.60912\bar{d}^2A^5 - 5.22277\bar{k}^2A^9)\end{aligned} \tag{A.1}$$

Phase portraits generated by numerical integration of the slow flow have been used to predict the qualitative behavior of ion motion near the stability boundary in the presence of nonlinearities. The presence of positive even multipoles was seen to cause early ejection and negative even multipoles to cause delayed ejection of ions. Independently present odd multipoles of either sign have the same effect as negative even multipoles in causing delayed ejection.

While our present study has served to reinforce conclusions arrived at by earlier workers who focussed on the influence of field inhomogeneities causing delayed ejection in mass selective boundary ejection experiments, it offers a few new insights.

First, we now have a better understanding on the role of hexapole superposition, specifically to the way in which its sign is important in discussion of ion dynamics at the boundary. To re-iterate our observation, the common perception is that the dynamics is unaffected if $\bar{h}$ changes sign. We report that the dynamics is unaffected if $\bar{h}$ and $\bar{d}$ change sign simultaneously but not otherwise (assuming both $\bar{h}$ and $\bar{d}$ are nonzero). Furthermore, when $\bar{d} = 0$, the sign-independence of the dynamics on $\bar{h}$ holds up to even the next order in the analysis (going beyond Franzen et al. [36]).

A second important contribution that the present study makes is to trap designers. As mentioned in our introductory remarks in this paper, newer trap geometries are under current investigation and their design optimization is performed either empirically or through numerical simulations. These techniques do not lend themselves to easily summarizing the effects of a large number of possible parameter variations. Considering that calculation of multipole contribution to the field within the trap cavity for a specified trap geometry is fairly routine and straightforward, inserting the weights of multipole superpositions for these geometries in the slow flow will enable easy visualization of ion dynamics at different q_z values in the neighborhood of the nominal stability boundary. This will help designers in understanding the effects of specific combinations of multipole superpositions in mass analyzers being investigated by them for use in mass selective boundary ejection experiments.

Acknowledgement

We gratefully acknowledge three anonymous reviewers for their comments and suggestions.

Appendix A. Fourth order MMS slow flow

The slow flow equation after carrying out the fourth order multiple scales analysis will be in the form:

Note that higher order MMS gives non-unique results (due to arbitrariness in the choice of X_1 in Eq. (23)). Moreover, due to harmonic balance approximations, the numerical coefficients above are not exact. However, the spirit of the calculation is correct in principle and a useful approximation is obtained, and so these terms are reported here for record.

Appendix B. Choice of time scales in MMS

Time scales chosen in the MMS when applied to Eq. (9) are $T_0 = \tau$, $T_1 = \sqrt{\epsilon}\tau$, $T_2 = \epsilon\tau$, ... Our choice is based on the following.

We consider:

$$\frac{\mathrm{d}^2x}{\mathrm{d}\tau^2} + 2(q_z^* + \epsilon\Delta)\,\cos(2\tau)(x + \epsilon x^3) = 0, \tag{B.1}$$

which can be rewritten as

$$\frac{\mathrm{d}^2x}{\mathrm{d}\tau^2} + 2q_z^*\,\cos(2\tau)x + 2\epsilon\,\cos(2\tau)(q_z^*x^3 + \Delta x) + \mathcal{O}(\epsilon^2) = 0. \tag{B.2}$$

We numerically integrate Eq. (B.2), neglecting $\mathcal{O}(\epsilon^2)$ terms, with initial conditions $x(0) = 0.01$ and $\dot{x}(0) = 0$ for a fixed value of $\epsilon = 0.001$. We observe the period of the slowly varying amplitude to be $T = 433.25$ (Fig. B.1(a)). With the same initial conditions, we integrate Eq. (B.2) again, but now for $\epsilon = 0.002$. This time period of the solution is observed to be $T = 306.35$.

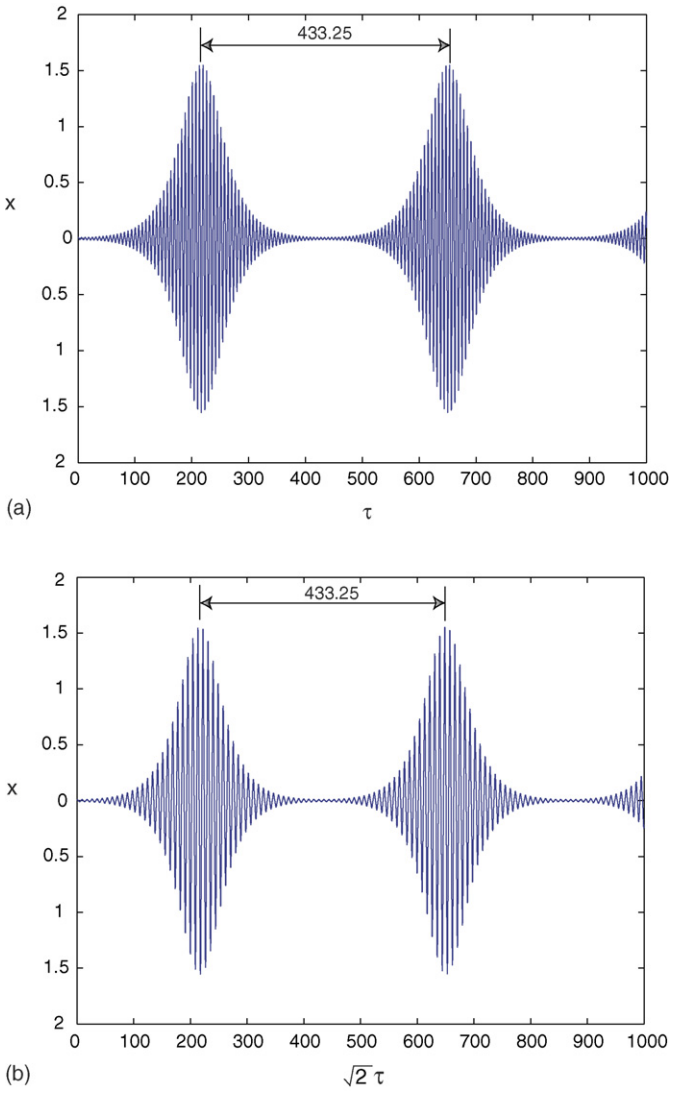

Fig. B.1. Time period of the amplitude for (a) $\epsilon = 0.001$ and (b) $\epsilon = 0.002$.

Note that $433.25/306.35 \approx 1.414\ldots \approx \sqrt{2}$. The solution for $\epsilon = 0.002$ is therefore plotted against $\sqrt{2}\tau$ instead of τ and we get approximately the same period, i.e., $T \approx 433.25$ (Fig. B.1(b)). This observation suggests that the $\sqrt{\epsilon}\tau$ time scale is present in the solution. We support our observation further using an analogy. The unperturbed equation in case of Eq. (9) is

$$\frac{d^2x}{d\tau^2} + 2q_z^* \cos(2\tau)x = 0. \tag{B.3}$$

This equation is a linear Mathieu equation with q_z^* value corresponding to q at the stability boundary. Eq. (B.3) has two linearly independent solutions, one periodic with constant amplitude and the other with amplitude growing linearly with time.

Now consider

$$\frac{d^2x}{d\tau^2} = 0. \tag{B.4}$$

It is a second order, linear homogeneous ordinary differential equation. It has two linearly independent solutions, one constant and the other linearly growing with respect to time, similar at an abstract level to the behavior of the amplitude for the linear Mathieu equation. If we perturb Eq. (B.4) as

$$\frac{d^2x}{d\tau^2} + \epsilon x = 0, \tag{B.5}$$

the solution becomes

$$x = A\ \cos(\sqrt{\epsilon}\ \tau) + B\ \sin(\sqrt{\epsilon}\ \tau), \tag{B.6}$$

where A and B depend upon the initial conditions. We see that time scale $\sqrt{\epsilon}\tau$ is present in the solution.

Eq. (9) is a perturbation to Eq. (B.3). So we expect time scales τ, $\sqrt{\epsilon}\tau$, $\epsilon\tau$, ... to be present in the solution. The final MMS approximation, of course, is amply supported by full numerical checks.

Appendix C. Expressions for X_1 and X_2

The solution for X_1 (not displaying the coefficients which are less than 10^{-5}) is:

$$\begin{aligned}
X_1 \approx\ & -1.13522\frac{\partial A}{\partial T_1}\sin\ T_0 - 0.18287\frac{\partial A}{\partial T_1}\sin(3T_0) \\
& - 0.00812\frac{\partial A}{\partial T_1}\sin(5T_0) - 0.00017\frac{\partial A}{\partial T_1}\sin(7T_0) \\
& - 0.60164\bar{h}A^2\ \cos(2\,T_0) - 0.6719\bar{d}A^4\ \cos(2T_0) \\
& + 0.00066\bar{h}A^2\ \cos(4T_0) + 0.00455\bar{d}A^4\ \cos(4T_0) \\
& + 0.00268\bar{h}A^2\ \cos(6T_0) + 0.0078\bar{d}A^4\ \cos(6T_0) \\
& + 0.00016,\ \bar{h}A^2\ \cos(8T_0) + 0.00116\bar{d}A^4\ \cos(8T_0) \\
& + 0.00011\bar{d}A^4\ \cos(10T_0) - 2.07004\bar{d}A^4 - 1.88307\bar{h}A^2
\end{aligned} \tag{C.1}$$

The solution for X_2 (not displaying the coefficients which are less than 10^{-5}) is:

$$\begin{aligned}
X_2 \approx\ & 1.1332\bar{h}A\frac{\partial A}{\partial T_1}\ \sin(2T_0) + 2.46062\bar{d}A^3\frac{\partial A}{\partial T_1}\ \sin(2T_0) \\
& - 0.00693\bar{h}A\frac{\partial A}{\partial T_1}\ \sin(4T_0) + 0.03699\bar{d}A^3\frac{\partial A}{\partial T_1}\ \sin(4T_0) \\
& - 0.00963\bar{h}A\frac{\partial A}{\partial T_1}\ \sin(6T_0) - 0.03737\bar{d}A^3\frac{\partial A}{\partial T_1}\ \sin(6T_0) \\
& - 0.00066\bar{h}A\frac{\partial A}{\partial T_1}\ \sin(8T_0) - 0.00662\bar{d}A^3\frac{\partial A}{\partial T_1}\ \sin(8T_0) \\
& - 0.00002\bar{h}A\frac{\partial A}{\partial T_1}\sin(10T_0) - 0.00073\bar{d}A^3\frac{\partial A}{\partial T_1}\sin(10T_0) \\
& - 0.00006\bar{d}A^3\frac{\partial A}{\partial T_1}\sin(12T_0) + 0.14628\Delta A\ \cos(3T_0) \\
& - 0.02631\bar{h}^2A^3\ \cos(3T_0) - 0.00325\bar{f}A^3\ \cos(3T_0) \\
& - 0.00009\bar{f}A^5\ \cos(3T_0) - 0.00195\bar{h}\bar{d}A^5\ \cos(3T_0) \\
& + 0.02946\bar{d}^2A^7\ \cos(3T_0) + 0.00187\Delta A\ \cos(5T_0) \\
& - 0.02469\bar{h}^2A^3\ \cos(5T_0) + 0.01234\bar{f}A^3\ \cos(5T_0)
\end{aligned}$$

$$
\begin{aligned}
&-0.15887\bar{h}\bar{d}A^5\ \cos(5T_0) + 0.01857\bar{f}A^5\ \cos(5T_0)\\
&-0.1447\bar{d}^2A^7\cos(5T_0) + 0.00007\Delta A\ \cos(7T_0)\\
&-0.00159\bar{h}^2A^3\ \cos(7T_0) + 0.00186\bar{f}A^3\cos(7T_0)\\
&-0.02564\bar{h}\bar{d}A^5\ \cos(7T_0) + 0.00456\bar{f}A^5\ \cos(7T_0)\\
&-0.02621\bar{d}^2A^7\ \cos(7T_0) - 0.00001\bar{h}^2A^3\ \cos(9T_0)\\
&+0.00015\bar{f}A^3\ \cos(9T_0) - 0.00231\bar{h}\bar{d}A^5\ \cos(9T_0)\\
&-0.000728\bar{f}A^5\ \cos(9T_0) - 0.00246\bar{d}^2A^7\ \cos(9T_0)\\
&-0.00013\bar{h}\bar{d}A^5\ \cos(11T_0) + 0.00009\bar{f}A^5\ \cos(11T_0)\\
&-0.00011\bar{d}^2A^7\ \cos(11T_0) \qquad \text{(C.2)}
\end{aligned}
$$

X_1 and X_2 are provided here with numerical coefficients of their terms truncated to five decimal places. In our calculations using MAPLE, more digits were retained.

Appendix D. Comparison of second order slow flow with beat envelope equation of Sudakov [22]

We reproduce Sudakov's equation of ion motion (Eq. (9) in Ref. [22]) below:

$$
\begin{aligned}
&\frac{\mathrm{d}^2u}{\mathrm{d}\xi^2} + 2q_0\ \cos(2\xi)u\\
&\quad = 2(q_0 - q)\cos(2\xi)u - q\ \cos(2\xi)4\alpha_4u^3, \qquad \text{(D.1)}
\end{aligned}
$$

where $u = z/z_0$, $\xi = \Omega t/2$ (= τ, in our study), $q_0 = q_z^*$ (in our study), $\alpha_4 = f(z_0^2/r_0^2)$ (= $\epsilon(\bar{f}/2)(z_0^2/r_0^2)$, in our study). The solution to Eq. (D.1) is assumed to be of the form (Eq. (A.1) in Sudakov [22]):

$$
\begin{aligned}
u(\xi) &= \epsilon Zu_1(\xi) + \epsilon^2(h_1\ \sin(\xi) + h_3\ \sin(3\xi) + \ldots)\\
&\quad + \epsilon^3(g_3\ \cos(3\xi) + g_5\ \cos(5\xi) + \ldots), \qquad \text{(D.2)}
\end{aligned}
$$

where Z is the beat envelope (our "amplitude") and u_1 is the periodic solution of the linear Mathieu equation at the stability boundary and h_k's and g_k's are slowly varying amplitudes of the harmonics.

The beat envelope equation has been found by Sudakov [22] to be

$$
\frac{\mathrm{d}^2Z}{\mathrm{d}\xi^2} + 0.8873(q_0 - q)Z - 1.4572\alpha_4Z^3 = 0. \qquad \text{(D.3)}
$$

However, the slow flow equation (Eq. (34)) derived by us, when there is only octopole nonlinearity, has the form:

$$
\ddot{A} = \epsilon(0.8773\Delta A + 0.8897\bar{f}A^3). \qquad \text{(D.4)}
$$

We must now transform our equation, Eq. (D.4), to the form presented by Sudakov [22]. This will require transforming different parameters in our equation to conform to Eq. (D.3). This is described below.

We nondimensionalized the axial position variable z as $x = z/r_0$; since $u = z/z_0$, we have $x = (z_0/r_0)u$. Since $x = X_0 + \mathcal{O}(\sqrt{\epsilon}) = A\xi_1 + \mathcal{O}(\sqrt{\epsilon})$, we write $x \approx A\xi_1$, i.e., $(z_0/r_0)u \approx A\xi_1$. Sudakov shows in Appendix A of Ref. [22] that his h_k's and g_k's are of the first and second orders, respectively. Since ϵ is a book-keeping parameter in that study (the correspondence between Sudakov's ϵ and ours is therefore not direct, and is avoided in this discussion), we can write $u \approx Zu_1$, and therefore $A \approx (z_0/r_0)(u_1/\xi_1)Z$. Finally, substituting $\bar{f} = (2/\epsilon)(r_0^2/z_0^2)\alpha_4$, $\Delta = -(q_0 - q)/\epsilon$ and $A \approx (z_0/r_0)(u_1/\xi_1)Z$ into Eq. (D.4), we obtain:

$$
\frac{\mathrm{d}^2Z}{\mathrm{d}\xi^2} + 0.8873(q_0 - q)Z - 1.7794\left(\frac{u_1}{\xi_1}\right)^2\alpha_4Z^3 = 0. \qquad \text{(D.5)}
$$

From Eq. (10) of Sudakov [22], it can be seen that u_1 is scaled such that all coefficients in the solution add to 1. In our study, we have not imposed this condition on ξ_1 and we have obtained, instead, $u_1/\xi_1 = 0.90495$. Substituting this, Eq. (D.5) then becomes:

$$
\frac{\mathrm{d}^2Z}{\mathrm{d}\xi^2} + 0.8873(q_0 - q)Z - 1.4572\alpha_4Z^3 = 0 \qquad \text{(D.6)}
$$

Comparing Eq. (D.3) and Eq. (D.6) indicates that, for octopole superposition, the beat envelope equation and the slow flow are identical.

We next investigate the two equations (ours, and Sudakov's) for the case of hexapole superposition. Eq. (B.6) in Sudakov [22] which represents the beat envelope for hexapole superposition is:

$$
\frac{\mathrm{d}^2Z}{\mathrm{d}\xi^2} + 0.8873(q_0 - q)Z + 12.692\alpha_3^2Z^3 = 0. \qquad \text{(D.7)}
$$

Following the procedure adopted for octopole nonlinearity and substituting $\bar{h} = (3/2\sqrt{\epsilon})(r_0/z_0)$ in the slow flow, Eq. (34) with only hexapole superposition can be transformed to:

$$
\frac{\mathrm{d}^2Z}{\mathrm{d}\xi^2} + 0.8873(q_0 - q)Z + 7.1693\alpha_3^2Z^3 = 0. \qquad \text{(D.8)}
$$

It is observed that the coefficient of $\alpha_3^2Z^3$ in Eqs. (D.7) and (D.8) differ significantly. We now verify the correctness of the coefficients by comparing the solutions of the two equations with the solution of the original equation (Eq. (B.1)) in Sudakov

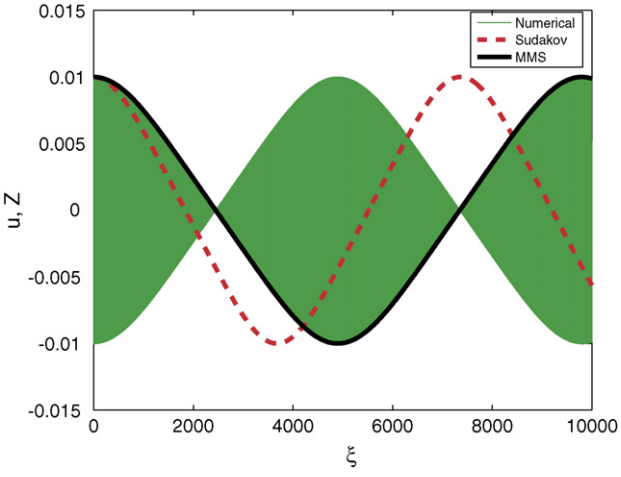

Fig. D.1. Comparison between amplitude obtained by (Eq. (D.8)) and Eq. (D.7) for $\alpha_3 = 0.02828$ (4% hexapole), $q = q_0 = 0.908046$, $u(0) = 0.01$, $\dot{u}(0) = 0$, $Z(0) = 0.01$, $\dot{Z}(0) = 0$.

[22] with hexapole superposition, which is:

$$\frac{d^2u}{d\xi^2} + 2q\cos(2\xi)u = -q\cos(2\xi)3\alpha_3 u^2. \quad \text{(D.9)}$$

These equations are integrated using the ODE45 routine of MATLAB with tolerance values of 10^{-10}. The amplitude obtained from the transformed slow flow (Eq. (D.8)), shown as a heavy line in Fig. D.1, follows the solution of Eq. (D.1) very closely, while the amplitude from the beat envelope equation of Sudakov [22], Eq. (D.7), shown as a dash line in Fig. D.1, shows an error in the numerical term reported in Sudakov [22].

Appendix E. Initial condition calculation

We describe a procedure to obtain initial conditions for Eq. (34), correct up to $\mathcal{O}(\sqrt{\epsilon})$, from the initial conditions used to integrate Eq. (9).

We assume $X(0) = X_0(0)$. Since $X_0 = A(T_1)\,\xi_1(T_0)$, we have:

$$X_0(0) = A(T_1)\,\xi_1(0).$$

From the expression for X_0 obtained from MAPLE, we have $\xi_1(0) = 1.105$. Therefore, the initial condition for A is:

$$A(0) = \frac{X_0(0)}{1.105} + \mathcal{O}(\sqrt{\epsilon}) = \frac{X(0)}{1.105} + \mathcal{O}(\sqrt{\epsilon}).$$

We also have

$$\begin{aligned}\dot{X}(0) &= \dot{X}_0(0) + \sqrt{\epsilon}\,\dot{X}_1(0) + \mathcal{O}(\epsilon)\\ &= \xi_1(0)\dot{A}(0) + \sqrt{\epsilon}\,\frac{\partial X_1}{\partial T_0} + \mathcal{O}(\epsilon). \quad \text{(E.1)}\end{aligned}$$

From our solution (MAPLE), we have

$$\frac{\partial X_1}{\partial T_0} = -1.7244\frac{\partial A}{\partial T_1}.$$

Substituting the above in Eq. (34), we get

$$\dot{A}(0) = \frac{\dot{X}(0)}{-0.6193} + \mathcal{O}(\epsilon).$$

Note that some small errors remain for nonzero ϵ, in light of which some small adjustments in initial conditions are allowed to obtain better fits.

References

[1] P.H. Dawson, Quadrupole Mass Spectrometry and its Application, Elsevier, Amsterdam, 1976.
[2] R.D. Knight, Int. J. Mass Spectrom. Ion. Phys. 51 (1983) 127.
[3] R.E. March, R.J. Hughes, Quadrupole Storage Mass Spectrometry, Wiley–Interscience Publications, New York, 1989.
[4] N.W. McLachlan, Theory and Applications of Mathieu Functions, Oxford University Press, UK, 1947.
[5] G.C. Stafford, P.E. Kelley, J.E.P. Syka, W.E. Reynolds, J.F.J. Todd, Int. J. Mass Spectrom. Ion Process 60 (1984) 85.
[6] J.E.P. Syka, R.E. March, J.F.J. Todd (Eds.), Practical Aspects of Ion Trap Mass Spectrometry, CRC Press, New York, 1995, Chapter 4, p. 169.
[7] J.M. Wells, W.R. Plass, G.E. Patterson, Z. Ouyang, E.R. Badman, G.R. Cooks, Anal. Chem. 71 (1999) 3405.
[8] W.R. Plass, H. Li, R.G. Cooks, Int. J. Mass Spectrom. 228 (2003) 237.
[9] Y. Wang, J. Franzen, Int. J. Mass Spectrom. Ion Process 132 (1994) 155.
[10] J. Franzen, Int. J. Mass Spectrom. Ion Process 125 (1993) 165.
[11] Y. Wang, J. Franzen, K.P. Wanczek, Int. J. Mass Spectrom. Ion Process 124 (1993) 125.
[12] J. Franzen, Int. J. Mass Spectrom. Ion Process 130 (1994) 15.
[13] J.C. Schwartz, M.W. Senko, J.E.P. Syka, J. Am. Soc. Mass Spectrom. 13 (2002) 659.
[14] B.A. Collings, W.R. Stott, F.A. Londry, J. Am. Soc. Mass Spectrom. 14 (2003) 622.
[15] A.L. Michaud, A.J. Frank, C. Ding, X.Z. Zhao, D.J. Douglas, J. Am. Soc. Mass Spectrom. 16 (2004) 837.
[16] B.A. Collings, J. Am. Soc. Mass Spectrom. 16 (2005) 1342.
[17] D.B. Langmuir, R.V. Langmuir, H. Shelton, R.F. Wuerker, Containment device. US Patent 3,065,640, 1962.
[18] R.F. Bonner, J.E. Fulford, R.E. March, G.F. Hamilton, Int. J. Mass Spectrom. Ion Phys. 24 (1977) 255.
[19] M.G. Blain, L.S. Riter, D. Cruz, D.E. Austin, G. Wu, W.R. Plass, R.G. Cooks, Int. J. Mass Spectrom. 236 (2004) 91.
[20] D.E. Austin, D. Cruz, M.G. Blain, J. Am. Soc. Mass Spectrom. 17 (2006) 430.
[21] G. Wu, R.G. Cooks, Z. Ouyang, Int. J. Mass Spectrom. 241 (2005) 119.
[22] M. Sudakov, Int. J. Mass Spectrom. 206 (2001) 27.
[23] G.T. Abraham, A. Chatterjee, Nonlinear Dyn. 31 (2003) 347.
[24] E.C. Beaty, Phys. Rev. A 33 (1986) 3645.
[25] S. Sevugarajan, A.G. Menon, Int. J. Mass Spectrom. 218 (2002) 181.
[26] G.T. Abraham, A. Chatterjee, A.G. Menon, Int. J. Mass Spectrom. 231 (2004) 1.
[27] R.E. March, F.A. Londry, R.E. March, J.F.J. Todd (Eds.), Practical Aspects of Ion Trap Mass Spectrometry, CRC Press, New York, 1995 Chapter 2, p. 25.
[28] A.H. Nayfeh, Perturbation Methods, Wiley–Interscience Publications, New York, 1973.
[29] M.J. Holmes, Introduction to Perturbation Methods, Springer-Verlag, New York, 1991.
[30] E.J. Hinch, Perturbation Methods, Cambridge University Press, UK, 1991.
[31] J. Kevorkian, J.D. Cole, Multiple Scale and Singular Perturbation Methods, Applied Mathematical Sciences, vol. 114, Springer-Verlag, New York, 1996.
[32] J.J. Stoker, Non-linear Vibrations in Mechanical and Electrical Systems, Interscience Publishing, New York, 1950.
[33] A. Chatterjee, D. Chatterjee, Nonlinear Dyn. 46 (2006) 179.
[34] S.L. Das, A. Chatterjee, Nonlinear Dyn. 32 (2003) 161.
[35] K. Nandakumar, A. Chatterjee, Trans. ASME J. Vib. Acoustics 127 (2005) 416.
[36] J. Franzen, R.H. Gabling, M. Schubert, Y. Wang, R.E. March, J.F.J. Todd (Eds.), Practical Aspects of Ion Trap Mass Spectrometry, CRC Press, New York, 1995 Chapter 3, p. 49.